energies

MDPI

Article

Reactive Transport Modeling of CO_2-Brine–Rock Interaction on Long-Term CO_2 Sequestration in Shihezi Formation

Zhuo Li [1,2], Yanfang Lv [1,*], Bin Liu [3,*] and Xiaofei Fu [1]

[1] School of Earth Sciences, Northeast Petroleum University, Daqing 163318, China
[2] Office of Academic Research, Northeast Petroleum University, Daqing 163318, China
[3] School of Electrical Engineering and Information, Northeast Petroleum University, Daqing 163318, China
* Correspondence: 571128lyf@nepu.edu.cn (Y.L.); liubinnepu@163.com (B.L.)

Abstract: Carbon Capture and Storage (CCS) is attracting increasing scientific attention. Although experiments can explore the chemical process of CO_2 sequestration, they are limited in time. CO_2 geological storage will last hundreds and thousands of years, even much longer, so the numerical simulation method is used to conduct kinetic batch modeling and reactive transport modeling. The geochemical simulation tool—TOUGHREACT—is used to imitate CO_2-brine–rock interactions at the Shihezi Formation in the Ordos basin. The mechanisms of CO_2-brine–rock interaction and their effects on the reservoir are discussed, especially the change in structure and properties. K-feldspar and albite will dissolve as the main primary minerals. However, calcite and quartz will dissolve first and precipitate last. In addition, siderite and ankerite also appear as precipitation minerals. Mineral dissolution and precipitation will alter the formation of petrophysical parameters, such as porosity and permeability, which play significant roles in the geological storage environments. Although the CO_2-brine–rock interaction rate may be small, it is an ideal way of geological storage. Regardless of what minerals dissolve and precipitate, they will improve the dissolution of CO_2. The interaction between rock and brine with dissolved CO_2 can promote the amount of mineralization of CO_2, called mineral trapping, which has a positive effect on the long-term feasibility of CO_2 storage.

Keywords: CO_2 geological storage; reactive transport modeling; CO_2-brine–rock interaction

Citation: Li, Z.; Lv, Y.; Liu, B.; Fu, X. Reactive Transport Modeling of CO_2-Brine–Rock Interaction on Long-Term CO_2 Sequestration in Shihezi Formation. *Energies* **2023**, *16*, 670. https://doi.org/10.3390/en16020670

Academic Editors: João Fernando Pereira Gomes and Reza Rezaee

Received: 6 November 2022
Revised: 25 December 2022
Accepted: 3 January 2023
Published: 6 January 2023

1. Introduction

Greenhouse gases, especially CO_2, have increased rapidly and led to climate change with severe potential consequences. Novel technologies are proposed for carbon dioxide (CO_2) capture, storage, and utilization. For example, hydrogenation of CO_2 is an important representative among CO_2 utilization [1,2]. In addition, in situ catalytic hydrogenation of CO_2 during steam-based enhanced oil recovery not only enhances the oil-recovery factor but also reduces CO_2 emission significantly [3]. Carbon Capture and Storage technology (CCS) is the best scheme to reduce carbon emissions under the condition of existing technological means, which is gradually attracting people's attention [4,5]. As an important part of CCS technology, the study of CO_2 geological storage is of great significance for the development of CCS technology [6]. At present, research institutions and scholars from the United States, Norway, Canada, Germany, Australia, China, and other countries have carried out various studies on CCS and achieved fruitful results [7,8]. Some commercial CO_2 geological sequestration projects in many countries have also been launched, a large amount of experience and field data have been accumulated in CCS engineering, and some important progresses have been made [9]. Europe and North America have carried out CCS projects since the 1990s, such as Norway, Canada, and the United States. Australia and New Zealand are not far behind. China's CCS research started relatively late, and there is still some gap with the international advanced level [10–12].

According to the criteria given by the IPCC, the site for CO_2 sequestration should be guaranteed to remain more than 99% (probability greater than 90%) after 100 years

and more than 99% (probability greater than 66%) after 1000 years. Although some key factors of caprock are essential to judge whether the storage site is safe, the influence of CO_2 injection on reservoirs cannot be ignored either [13–16]. Therefore, it is of great significance to study the influence of CO_2 injection on reservoirs. CO_2-brine-rock interactions are important for CO_2 migration and storage safety. The interaction type includes dissolution and precipitation. The former may lead to increases in porosity and permeability, which facilities CO_2 migration; the latter may lead to decreases in porosity and permeability, which may hinder CO_2 migration in porous media. For CO_2 sequestration safety, CO_2 can be mineralized in the form of carbonatite through CO_2-brine-rock interactions. It is the idealist storage mechanism in CO_2 geological storage.

At present, the research methods of CO_2-brine-rock reaction during CO_2 geological storage mainly include laboratory test and numerical simulation [17]. Results of the CO_2-brine-rock reaction and the influence on long-term CO_2 storage for reservoir performance can be directly observed by physical experiments, and the risk of leakage can be evaluated accordingly [11,12]. However, there are some limitations for laboratory investigation. On the one hand, it is almost impossible to simulate geological conditions in the laboratory, especially for long-term geochemical reactions. On the other hand, there are a limited number of natural cores to carry out experiments [18,19]. It is necessary to figure out effects of geochemical reactions on reservoir physical properties by numerical simulations.

"Coal-to-Liquid Chemical Exhaust Capture and Storage in Deep Saline Aquifer" was the first CCS project in China [10], which was a whole-process demonstration project. This project was implemented by the Shenhua Group that was a super-large coal enterprise ranking first in the world. The Shihezi Formation is one of the five target areas in the Ordos basin. We study changes in reservoir properties that are influenced by CO_2 injection. CO_2 migration, CO_2-brine-rock interaction, and their effects on the reservoir are investigated by numerical simulation. In particular, the influence of the CO_2-brine–rock reaction on reservoir physical properties is discussed on a large time scale, which provides theoretical guidance for long-term safe CO_2 storage projects.

2. CO2 Storage Area and Major Interactions

2.1. Background

Geological formations, used for large volumes of CO_2 storage, can be categorized: saline aquifer formations, depleted oil and gas reservoirs, storage as a part of CO_2 EOR projects, coal bed storage, and other formations including volcanic rocks (especially basalt) and underground caverns. The first two are the main classes of these porous reservoirs. Generally, CO_2 storage sites need to be deeper than 800 m to ensure that CO_2 is in a dense form as a super-critical phase. At a depth of around 1 km or more, the reservoir potentially contains low-permeably sealing units for long-term trapping of CO_2.

The most distinctive feature is porousness and high permeability in the reservoir of the Ordos basin, where not only are oil, gas, and coal resources abundant, but the brine is also widely distributed. This means that there is tremendous potential for CO_2 sequestration. Based on the analysis of strata in the Ordos basin, the northeastern part of the basin has the geological conditions for CO_2 storage and has been chosen as the target area for CCS. Now, the first CCS demonstration and storage basin of China has been built in the Ordos basin [10].

Based on domestic and foreign CO_2 storage experience, the existing geological data, and stratigraphic characteristics, there are five candidate areas for CO_2 storage in the Ordos Basin: Triassic Liujiagou Formation reservoir-caprock association, Permian Shiqianfeng Formation reservoir-caprock association, Permian Shihezi Formation reservoir-caprock association, Permian Shanxi Formation reservoir-caprock association, and Ordovician Majiagou Formation reservoir-cap association. The reservoir types of the above five reservoir-cap assemblages are all sandstone, with the highest content of quartz as the reservoir mineral. Geological data of the numerical model are from the Shihezi Formation [10].

2.2. Numerical Model and Kinetics of CO_2-Brine-Rock Interaction

2.2.1. Description of Numerical Model

The numerical models are based on the Shihezi Formation in the Ordos Basin, whose data are from the real geological data. The depth of the storage site is between 1650 m and 1850 m, the formation pressure is 16.5 MPa, and the temperature is 55–75 °C. The CO_2 migration process in the reservoir is described in a 2D model. At the same time, CO_2-brine-rock interactions, including dissolution or precipitation, are simulated to investigate changes in minerals in the reservoir, as well as both porosity and permeability. The model thickness of the reservoir is 100 m, and the longitude distance is 5 km. The CO_2 injection well is located at the lower left, as shown in Figure 1. Vertically, it is divided into 20 layers, and the mesh size of each layer is 5 m. In the lateral direction, there are 51 grids, and the grid size increases gradually from left to right. The number of grids is 1020 in total in the conceptual model.

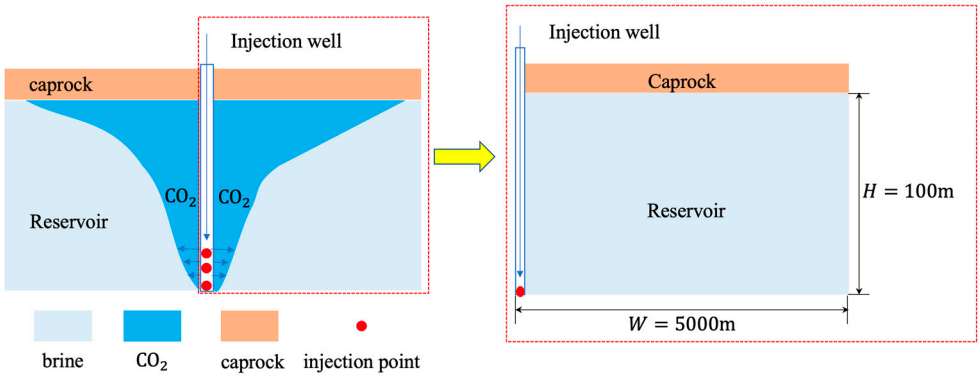

Figure 1. The conceptual model of numerical simulation.

2.2.2. Kinetics of CO_2-Brine-Rock Interaction

To represent a geochemical system, a subset of N_C aqueous species are selected as the basis species, while other ones are called secondary species including aqueous complexes, precipitated minerals, and gaseous species [20]. In TOUGHREACT, the kinetic rate is calculated according to basis species that are used to describe the CO_2-brine-rock interaction [21]:

$$r_n = f(c_1, c_2, \cdots, c_{N_C}) = \pm k_n A_n \left|1 - \Omega_n^{\theta}\right|^{\eta}, n = 1, 2, \cdots, N_q$$

where r_n is positive representing mineral precipitation, and negative represents dissolution. A_n stands for the specific reactive surface area. Ω_n is the kinetic saturation of reactive mineral, and can be calculated by $\Omega_n = K_n^{-1} \prod c_j^v \gamma_j^v$, where K_n is the equilibrium constant of the n-th mineral, and c_j^v and γ_j^v are the molar concentration and thermodynamic activity coefficient of j-th basis species in the v-th aqueous complex, respectively. Parameters of both θ and η are usually set to 1. The kinetic rate constant k_n can be calculated by the following equation:

$$k = k_{25} \cdot \exp\left[\frac{E_a}{R}\left(\frac{1}{T} - \frac{1}{298.15}\right)\right]$$

where k_{25} is the kinetic rate constant at 25 °C (mol/m^{2}s), E_a is the activation energy (J/mol), R is the gas constant (8.31 J/mol K), and T is the temperature (K).

The above equation can be expressed in a more complicated form:

$$k = k_{25}^n \cdot \exp\left[\frac{-E_a^n}{R}\left(\frac{1}{T} - \frac{1}{298.15}\right)\right] + k_{25}^{H^+} \cdot \exp\left[\frac{-E_a^{H^+}}{R}\left(\frac{1}{T} - \frac{1}{298.15}\right)\right] a_{H^+}^{n_{H^+}} + k_{25}^{OH^-} \cdot \exp\left[\frac{-E_a^{OH^-}}{R}\left(\frac{1}{T} - \frac{1}{298.15}\right)\right] a_{OH^-}^{n_{OH^-}}$$

where n, H^+, and OH^- stand for the neutral, acid, and base mechanism, respectively; E_a^n, $-E_a^{H^+}$, and $-E_a^{OH^-}$ are the corresponding activity energies; k_{25}^n, $k_{25}^{H^+}$, and $k_{25}^{OH^-}$ are kinetic rate constants at 25 °C; $a_{H^+}^{n_{H^+}}$ and $a_{OH^-}^{n_{OH^-}}$ are activities of H^+ and OH^-, respectively, calculated by $a_{H^+}^{n_{H^+}} = \gamma_{H^+}c_{H^+}$ and $a_{OH^-}^{n_{OH^-}} = \gamma_{OH^-}c_{OH^-}$, where γ_{H^+}, c_{H^+}, γ_{OH^-}, and c_{OH^-} are thermodynamic activity coefficients and molar concentrations of H^+ and OH^-, respectively. For CO_2 sequestration, the acidity and basicity of brine in the reservoir will vary, which will result in different reactions for acid and base mechanisms.

2.3. Parameters of Numerical Simulation and Geochemical Interactions

The reservoir is modeled as porous media, the parameters of which are detailed in Table 1. Core samples are from the Shihezi Formation in the Ordos basin, and geological model parameters are from [11], including the minerals content and brine composition. The minerals content data are listed in Table 2, and the brine composition is listed in Table 3. The injection period is 30 years, and the simulation time is 2000 years. Here, some primary minerals are chosen to analyze the sensitivity of the numerical model. Based on the content of alkali feldspar and plagioclase, we set four cases for sensitivity analysis, which are classified by the compositions and contents of primary minerals.

Table 1. Parameters of numerical model [22].

Parameter	Reservoir
Thickness (m)	100
Temperature (°C)	50
Pressure (MPa)	20.0
Density of rock (kg/m^3)	2400
Porosity (%)	12.0
Horizontal permeability (m^2)	5.47×10^{-15}
Vertical permeability (m^2)	5.47×10^{-15}
Liquid relative permeability	$k_{rl} = \begin{cases} \sqrt{S^*}\left\{1-\left(1-(S^*)^{\frac{1}{m}}\right)^m\right\}^2 & S_l < S_{ls} \\ 1 & S_l \geq S_{ls} \end{cases}$, $S^* = \frac{(S_l - S_{lr})}{(1-S_{lr})}$, $m = 0.457$, $S_{lr} = 0.300$
Gas relative permeability	$k_{rg} = \begin{cases} 1-k_{rl} & S_{gr} = 0 \\ (1-\hat{S})^2(1-\hat{S}^2) & S_{gr} > 0 \end{cases}$, $\hat{S} = \frac{(S_l - S_{lr})}{(1-S_{lr}-S_{gr})}$, $S_{gr} = 0.05$
Capillary pressure	$P_c = -P_0\left[(S^*)^{\frac{-1}{m}} - 1\right]^{1-m}$, $P_{max} \leq P_c \leq 0$, $m = 0.457$, $S_{lr} = 0.200$, $P_{max} = 1.00 \times 10^7$Pa, $P_0 7.71 \times 10^5$Pa,

Table 2. Minerals content [11].

No.	Minerals	Content1 (V%) Case 1	Content2 (V%) Case 2	Content3 (V%) Case 3	Content4 (V%) Case 4
1	quartz	60.44	60.44	60.44	60.44
2	K-feldspar	4.50	4.50	12.00	12.00
3	albite	12.50	6.50	6.00	12.00
4	anorthite	8.00	14.00	7.00	1.50

Table 2. *Cont.*

No.	Minerals	Content1 (V%) Case 1	Content2 (V%) Case 2	Content3 (V%) Case 3	Content4 (V%) Case 4
5	calcite	3.00	3.00	3.00	5.00
6	illite	4.50	4.50	2.00	2.00
7	smectite-Ca	1.25	0.50	2.5	1.25
8	smectite-Na	1.25	2.00	2.5	1.25
9	chlorite	4.56	4.56	4.56	4.56

Table 3. Brine composition [11].

Composition	Concentration (mol/L)	Composition	Concentration (mol/L)
Ca^{2+}	1.6113×10^{-1}	Cl^-	5.0558×10^{-1}
Na^+	1.6779×10^{-1}	NO_3^-	6.3000×10^{-4}
Mg^{2+}	8.2800×10^{-3}	HCO_3^-	1.0300×10^{-3}
K^+	6.3000×10^{-4}	SO_4^-	1.6980×10^{-4}
Fe^{2+}	1.6980×10^{-4}		

3. Discussion of Numerical Simulation

3.1. CO_2 Migration

CO_2 will migrate upward with buoyancy after injection, some of which will move into both sides laterally because of the performance of caprock overlying the formation. Gas saturation (Sg) is used to describe the distribution of gaseous CO_2 after injection into the formation, as shown in Figure 2. Simulation results in Sections 3.1–3.4 are based on Case 1. In the reservoir, Sg near the injection point in the vertical direction is much larger than the area far from the injection point. Once CO_2 is injected into the reservoir, gaseous CO_2 will migrate upward until reaching the caprock, and then spread in the lateral direction along caprock, as shown in Figure 2. During the CO_2 injection period, the horizontal distance is approximately 500 m, illustrated in Figure 2a. CO_2 will migrate horizontally and the largest distance from the injection point is about 600 m and a bit more, illustrated in Figure 2c,d. Moreover, the smaller the Sg value, the longer the time. During the migration of CO_2, the descending finger-like CO_2 distribution can be found from the region of the edge because the denser brine migrates downward. The reason is that CO_2 dissolves into the brine, which leads to greater brine density.

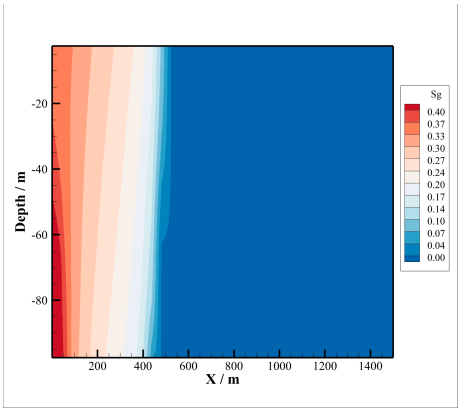

(**a**) 30 years

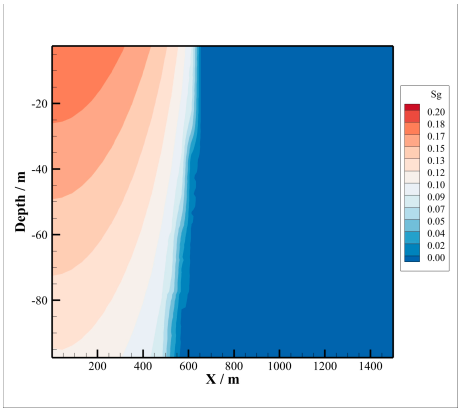

(**b**) 300 years

Figure 2. *Cont.*

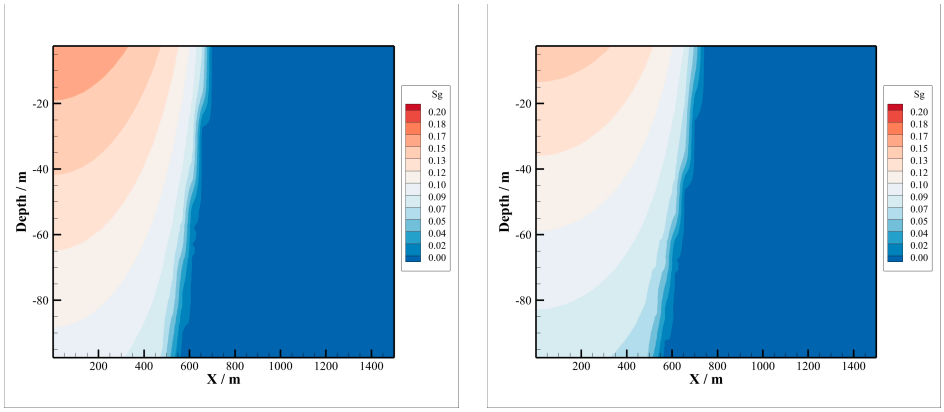

(**c**) 500 years (**d**) 1000 years

Figure 2. Sg since CO_2 injection.

The residual sequestration amount depends upon the maximal CO_2 saturation. The larger the gas saturation, the larger the CO_2 sequestration amount. Gaseous CO_2 content is greatly reduced in the reservoir by comparison among Figure 2a–d. On the one hand, massive CO_2 is dissolved into the brine, producing HCO_3^-, CO_3^{2-}, and H^+, which promotes reactions in porous media. On the other hand, CO_2-brine-rock interactions facilitate the CO_2 dissolution reversely.

The brine density will increase because of dissolved CO_2 and ions entering the solution resulting from minerals dissolution. The range of brine density variation is consistent with CO_2 gas saturation, as shown in Figure 3.

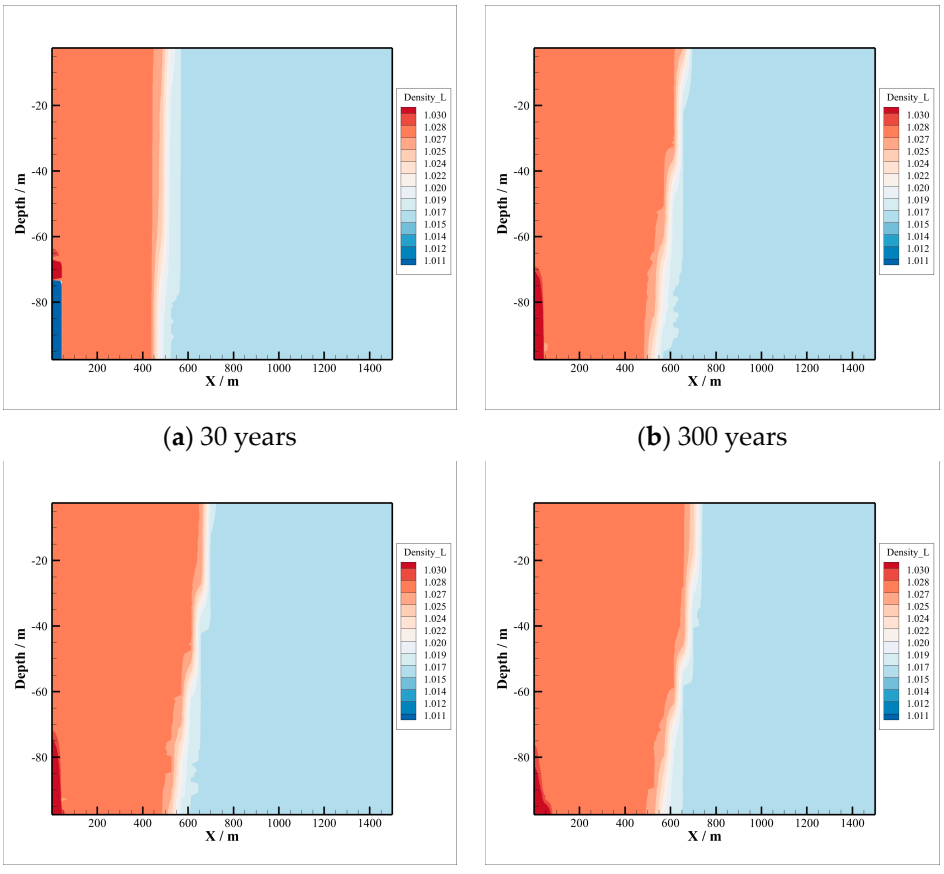

(**a**) 30 years (**b**) 300 years

(**c**) 500 years (**d**) 1000 years

Figure 3. Variations in brine density.

The density of the aqueous phase with dissolved CO_2 is calculated assuming the additivity of the volumes of brine and dissolved CO_2 as follows [20]:

$$\frac{1}{\rho_{aq}} = \frac{1 - X_3}{\rho_b} + \frac{X_3}{\rho_{CO_2}}$$

where X_3 is the mass fraction of CO_2 in the aqueous phase; ρ_{aq}, ρ_b, and ρ_{CO_2} are densities of aqueous, brine, and CO_2, respectively. The density of dissolved CO_2, ρ_{CO_2}, is a function of temperature and calculated by

$$\rho_{CO_2} = \frac{M_{CO_2}}{V_\phi} \times 10^3$$

where M_{CO_2} is the molecular weight of CO_2, and V_ϕ is the molar volume of dissolved CO_2:

$$V_\phi = a + bT + cT^2 + dT^3$$

in units of cm^3 per gram-mole, T is the temperature in °C, and a through d are fitting parameters: $a = 37.51$, $b = -9.585 \times 10^{-2}$, $c = 8.74 \times 10^{-4}$, and $d = -5.044 \times 10^{-7}$. Dissolved CO_2 is always dilute regardless of total fluid pressure, because it amounts at most to a few percent of total aqueous density. Accordingly, it is permissible to neglect the pressure dependence of the partial density of dissolved CO_2.

3.2. pH Value of Reservoir

The pH value decreases because of CO_2 dissolution, and the corresponding geochemical processes (Equations (1)–(3)) are listed as follows:

$$CO_{2(g)} + H_2O \leftrightarrow H_2CO_3 \quad (1)$$

$$H_2CO_3 \leftrightarrow H^+ + HCO_3^- \quad (2)$$

$$HCO_3^- \leftrightarrow H^+ + CO_3^{2-} \quad (3)$$

Figure 4 shows pH value distributions in the reservoir. CO_2 moves upward and diffuses around the injection well, where the pH value demonstrates this process due to CO_2 solution in reservoir. During the CO_2 injection period, CO_2 moves upward and spreads along the bottom of the caprock, where the pH value decreases. The CO_2 migration range in the reservoir top is almost the same as in the reservoir base since stopping injection. This is because of the lower permeability and higher residual gas saturation. In the reservoir base, the radius of the lateral migration region is about 600 m, while, in the top, it reaches 700 m. According to Figure 4b–d, pH values will increase over time. The main reason is geochemical interactions among CO_2, brine, and minerals in rock. These reactions will consume a large amount of CO_2, which will buffer the pH value of brine.

CO_2 dissolution will promote multiple complex physical and chemical processes, where there are super-critical CO_2 flow diffusion and convection, and many geochemical interactions with CO_2. In the reservoir, the geochemical process involves minerals dissolution and precipitation. On the one hand, the acidized brine will result in some minerals dissolving, such as calcite dissolution, whose geochemical processes equations are listed in (4)–(5):

$$CaCO_3 + CO_2 + H_2O \rightleftarrows CaHCO_3^+ + HCO_3^- \quad (4)$$

$$CaHCO_3^+ \rightarrow Ca^{2+} + HCO_3^- \quad (5)$$

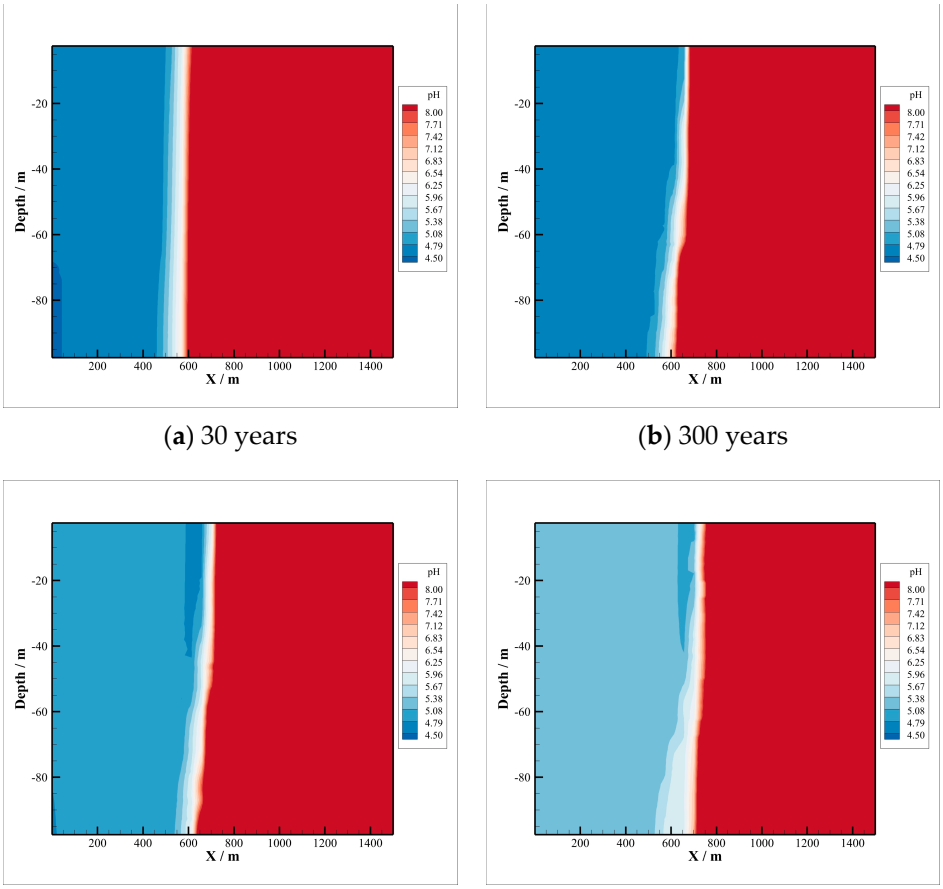

(**a**) 30 years (**b**) 300 years

(**c**) 500 years (**d**) 1000 years

Figure 4. Variations in pH in reservoir.

On the other hand, bicarbonate, and cations, such as Ca^{2+}, Mg^{2+}, Fe^{2+}, will produce carbonate eventually. These chemical processes are the main ways of CO_2 mineralization, and the corresponding geochemical processes equations are (6)–(8):

$$Ca^{2+} + HCO_3^- \rightarrow CaCO_{3(s)} + H^+ \quad (6)$$

$$Mg^{2+} + HCO_3^- \rightarrow MgCO_{3(s)} + H^+ \quad (7)$$

$$Fe^{2+} + HCO_3^- \rightarrow FeCO_{3(s)} + H^+ \quad (8)$$

3.3. Main Geochemical Interactions

At the first stage of injection, CO_2 will be stored in the free state in the reservoir. Hydrogen ions, induced by carbonic acid due to CO_2 dissolution, will reduce the pH value of brine, which will increase the reactivity of minerals and provide initial conditions for the CO_2-brine-rock reaction. Minerals dissolution and precipitation occur simultaneously. Dissolution is often observed first, and then precipitation. If minerals dissolution predominates, reservoir porosity will increase as well as its permeability. Otherwise, if the minerals precipitation plays a dominant role in reactions, the reservoir porosity will be weakened as well as its permeability. CO_2-brine-rock interaction can alter the mineral composition dramatically in the reservoir, and particularly have a significant influence on the reservoir pore structure, which will change the CO_2 storage capacity. In this numerical simulation, mineral dissolution and precipitation will be distinguished by negative and positive values, respectively, listed on the right side of the figures.

3.3.1. K-Feldspar

K-feldspar is the principal component of alkaline feldspar. In the laboratory, K-feldspar underwent only a weak dissolution and retained its crystalline form even in 100 °C [11]. However, K-feldspar dissolution can be observed on a large time scale in the numerical simulation. This means that in an acidic environment, it will be dissolved, as well as in CO_2 geological storage. The corresponding reaction equation is

$$\underbrace{KAlSi_3O_8}_{K-\text{feldspar}} + 4H^+ + 4H_2O \rightarrow K^+ + Al^{3+} + 3H_4SiO_4 \quad (9)$$

$$H_4SiO_4 \rightarrow SiO_2 + 2H_2O \quad (10)$$

Quartz will precipitate while K-feldspar dissolves, according to Equations (9) and (10), which is consistent with the SiO_2 content increase in Section 3.3.3. In Equation (9), H_4SiO_4 is in the form of hydrate and can be usually expressed as Equation (10).

K-feldspar dissolution can be modeled by numerical simulation, as shown in Figure 5. During the CO_2 injection period, there is only a little amount of dissolution, as shown in Figure 5a. The degree of K-feldspar dissolution increases gradually, as shown in Figure 5b–d. This means that a lot of CO_2 will be consumed by K-feldspar dissolution.

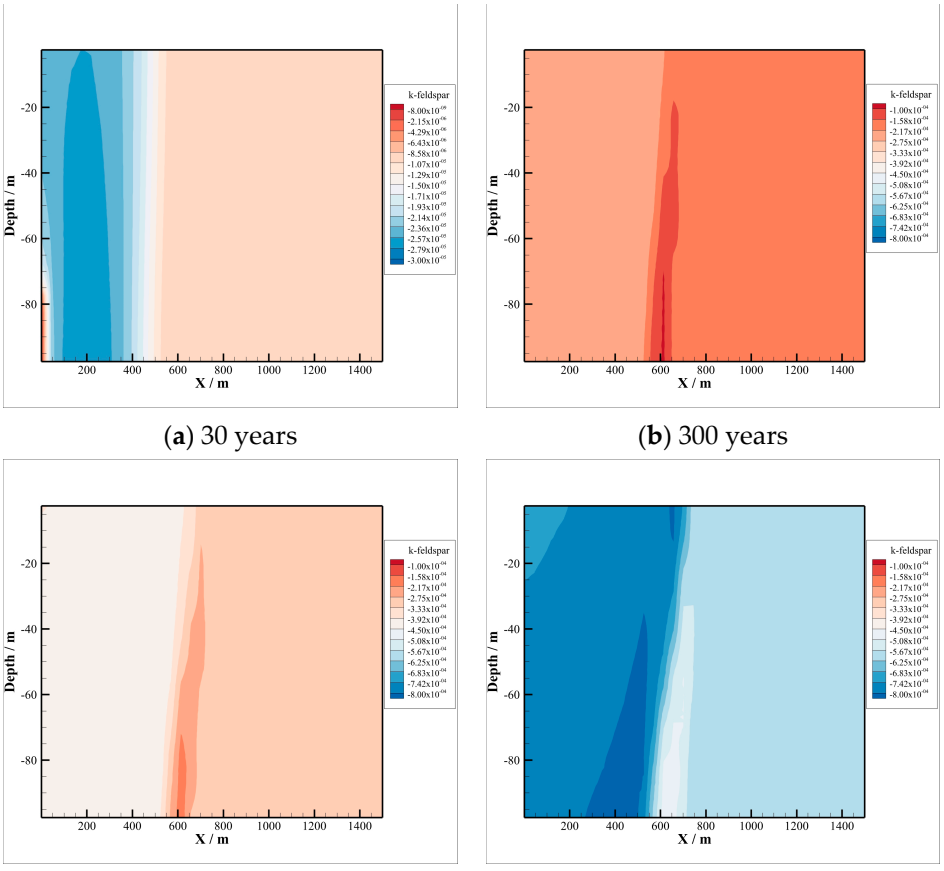

(**a**) 30 years (**b**) 300 years

(**c**) 500 years (**d**) 1000 years

Figure 5. K-feldspar dissolution.

3.3.2. Albite

Albite showed no noticeable dissolution at lower temperature and weak dissolution at higher temperature [11]. In the numerical simulation, there is no change in albite volume content. Otherwise, albite precipitation is observed after 500 years, as well as 1000 years, as shown in Figure 6. This is because a large amount of Al^{3+} is released by

K-feldspar dissolution, which will combine Na^+ in brine-forming albite precipitation. The amount of albite precipitation in the acidized environment is much less than in the neutral environment from the comparison between Figure 6a,b. Moreover, precipitated albite will transform another secondary mineral, dawsonite, which can be found in the simulation after 2000 years, and the corresponding chemical equation is

$$\underbrace{NaAlSi_3O_8}_{\text{albite}} + CO_2 + H_2O \rightleftarrows \underbrace{NaAlCO_3(OH)_2}_{\text{dawsonite}} + 3SiO_2 \quad (11)$$

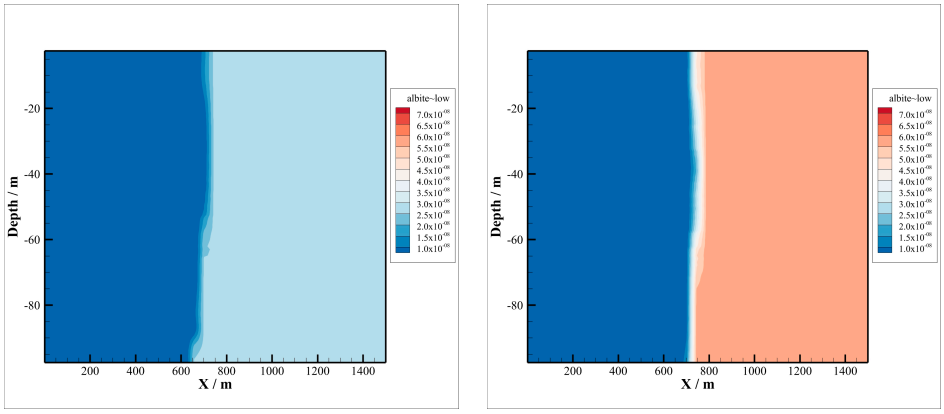

(**a**) 500 years (**b**) 1000 years

Figure 6. Albite precipitation.

Dawsonite does not always exist during the simulation period, which will dissolve after precipitation. The stability of dawsonite will be weakened with the increase in temperature.

3.3.3. Quartz

Quartz is commonly found in sand reservoirs, whose main chemical composition is SiO_2. It is difficult to observe quartz corrosion even at higher temperature. Some intense corrosion can be found at 250 °C [23]. In our simulation, there is little volume change during the first 30 years, as shown in Figure 7a. Quartz precipitation results in a volume content increase 300 years after injection, and the content continues to increase, as depicted in Figure 7b–d. The main reason of quartz precipitation is related to the dissolution of K-feldspar and albite, as illustrated in Equations (10) and (11).

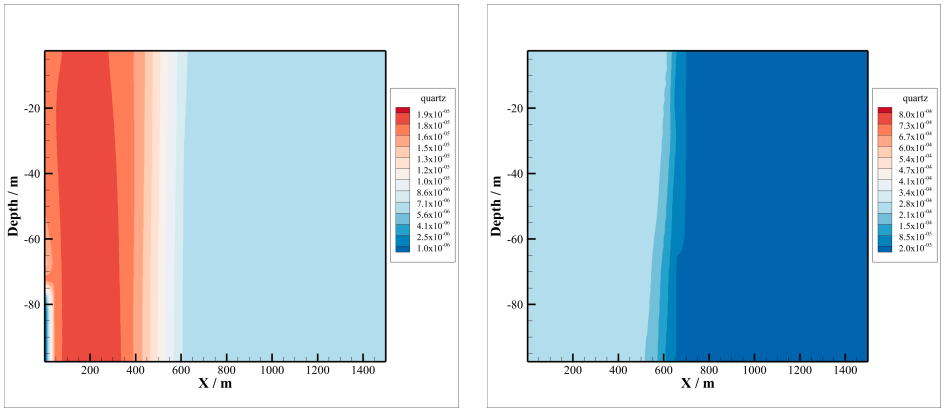

(**a**) 30 years (**b**) 300 years

Figure 7. *Cont.*

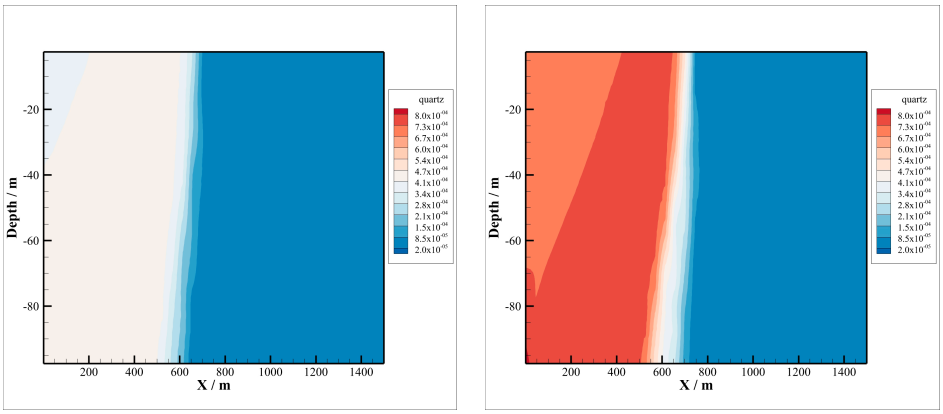

(**c**) 500 years (**d**) 1000 years

Figure 7. Quartz after CO_2 injection.

3.3.4. Calcite

Calcite is one of the most common carbonate minerals, which distributes widely in various geological environments. During the simulation, calcite dissolves in the range of CO_2 sequestration area and precipitates in the other areas, as shown in Figure 8. On the one hand, calcite dissolution in acidized brine can be described by chemical equations (Equations (4) and (5)). On the other hand, in a neutral environment, Ca^{2+} will combine with HCO_3^- or CO_3^{2-}, leading to calcite precipitation. This can be observed in Figure 8b-d, where some dark red areas are regions with the highest density of calcite precipitation.

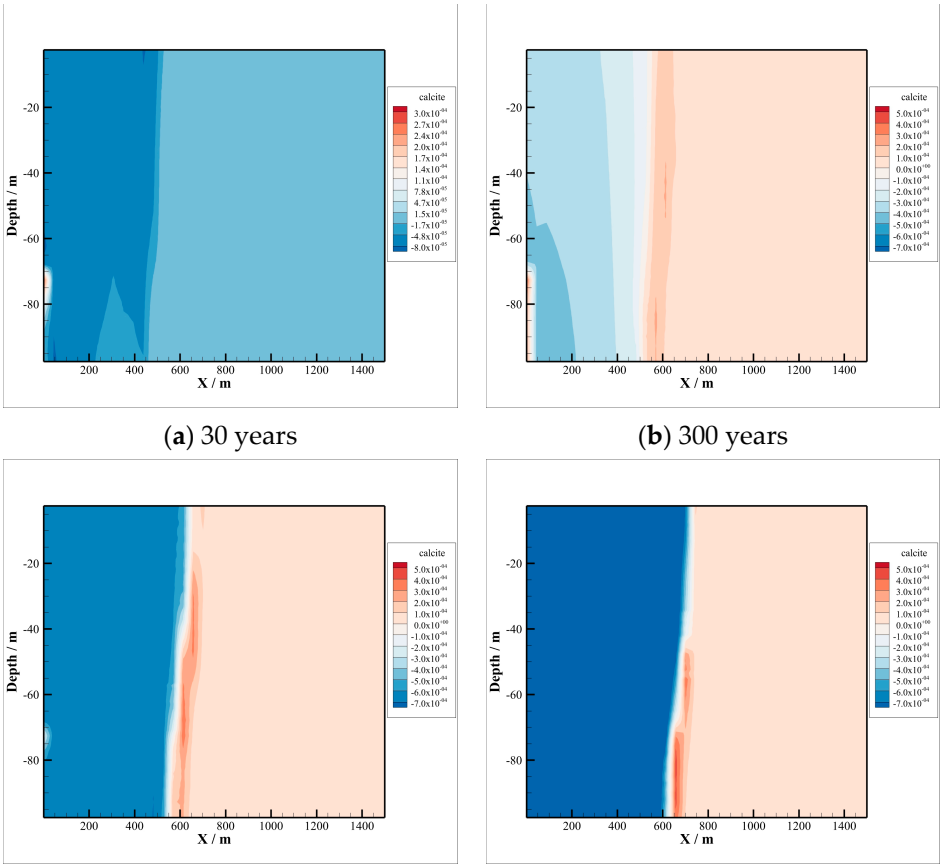

(**a**) 30 years (**b**) 300 years

(**c**) 500 years (**d**) 1000 years

Figure 8. Calcite dissolution and precipitation.

3.3.5. Other Minerals

Some other minerals precipitations can be found in the simulation, such as siderite and ankerite, as shown in Figures 9 and 10. It is the important way of CO_2 mineralization after CO_2 injection into the reservoir.

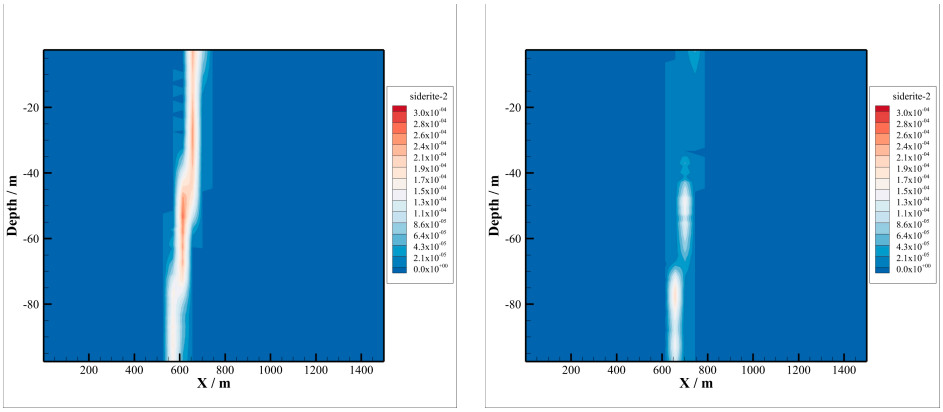

(**a**) 500 years (**b**) 1000 years

Figure 9. Siderite precipitation.

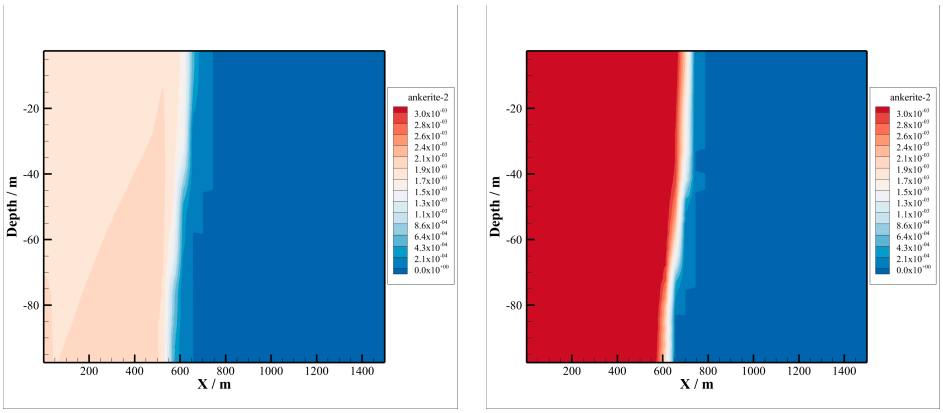

(**a**) 500 years (**b**) 1000 years

Figure 10. Ankerite precipitation.

Siderite is formed in the region between the CO_2 acidized area and neutral area. In this region, CO_2 dissolution into the brine will provide CO_3^{2-}, which will combine with Fe^{2+} to form siderite precipitation. In the CO_2 acidized area, siderite will dissolve because of the lower pH value. In the neutral area, there is not enough CO_3^{2-} to form precipitation. This is the main reason for siderite precipitation along the junction area. Ankerite precipitation can be found 500 years after injection. After that, a large amount of Ca^{2+} will be provided by calcite dissolution, and there is more ankerite precipitated in the higher-pH area than in the lower-pH area.

3.4. Porosity and Permeability

There are many methods to deal with the permeability variation of the reservoir. Here, the Kozeny-Carman equation is used to calculate the permeability value of the reservoir as the porosity changes [16]. There are some assumptions when dealing with this problem, such as the reservoir rock with uniform voids, ignoring the influence of rock particle size,

bending degree, and reaction surface area, whose changes have no effect on permeability. The Kozeny-Carman equation is listed as follows:

$$k = k_i \frac{(1-\phi_i)^2}{(1-\phi)^2} \left(\frac{\phi}{\phi_i}\right)^3 \tag{12}$$

where k_i and ϕ_i are the initial permeability and porosity, respectively. Variations in both porosity and permeability are illustrated in Figures 11 and 12, respectively, and the simulation time is 1000 years. The porosity will first increase and then decrease. The increase is due to primary minerals dissolution and the decrease is due to secondary minerals precipitation. According to Figures 11 and 12, their trends are almost the same, because the relationship between porosity and permeability is chosen as positively correlated.

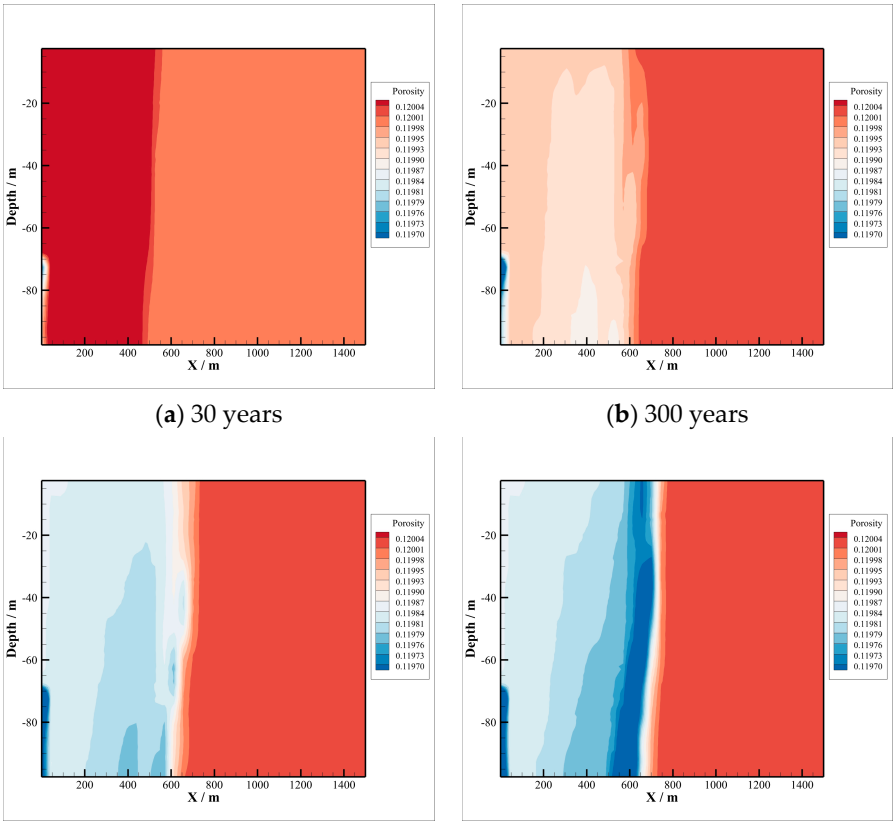

(**a**) 30 years (**b**) 300 years

(**c**) 500 years (**d**) 1000 years

Figure 11. Variations in porosity.

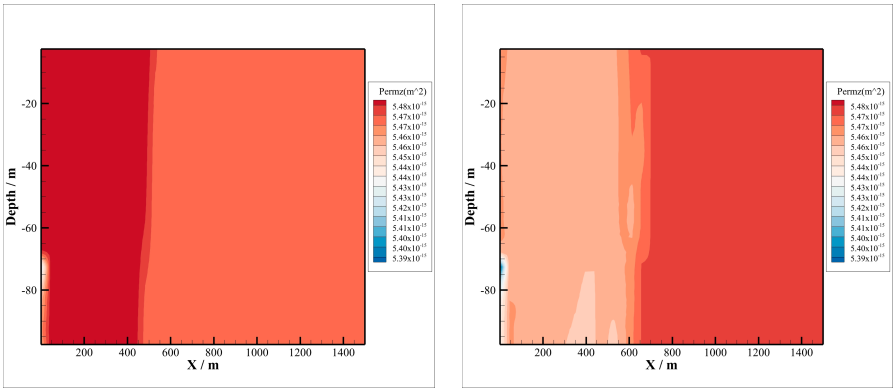

(**a**) 30 years (**b**) 300 years

Figure 12. *Cont.*

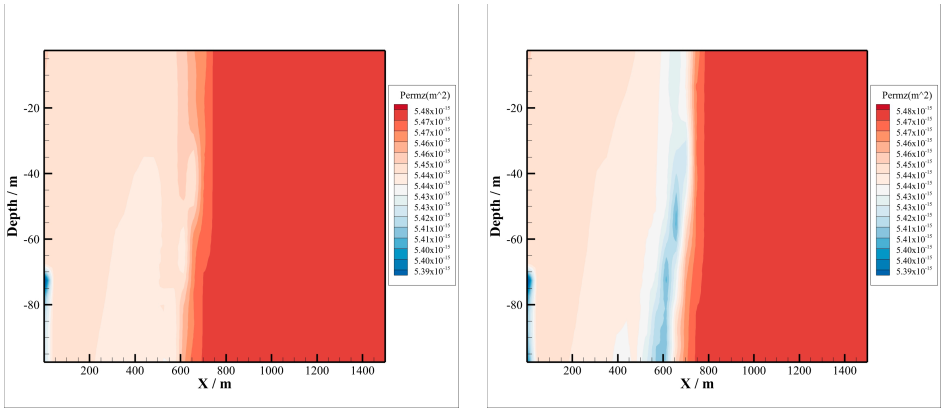

(**c**) 500 years (**d**) 1000 years

Figure 12. Variations in permeability.

3.5. Long-Term CO_2 Geological Storage

After 2000 years of CO_2 injection into the target area, the corresponding volume content changes of main minerals are shown in Figures 13–19.

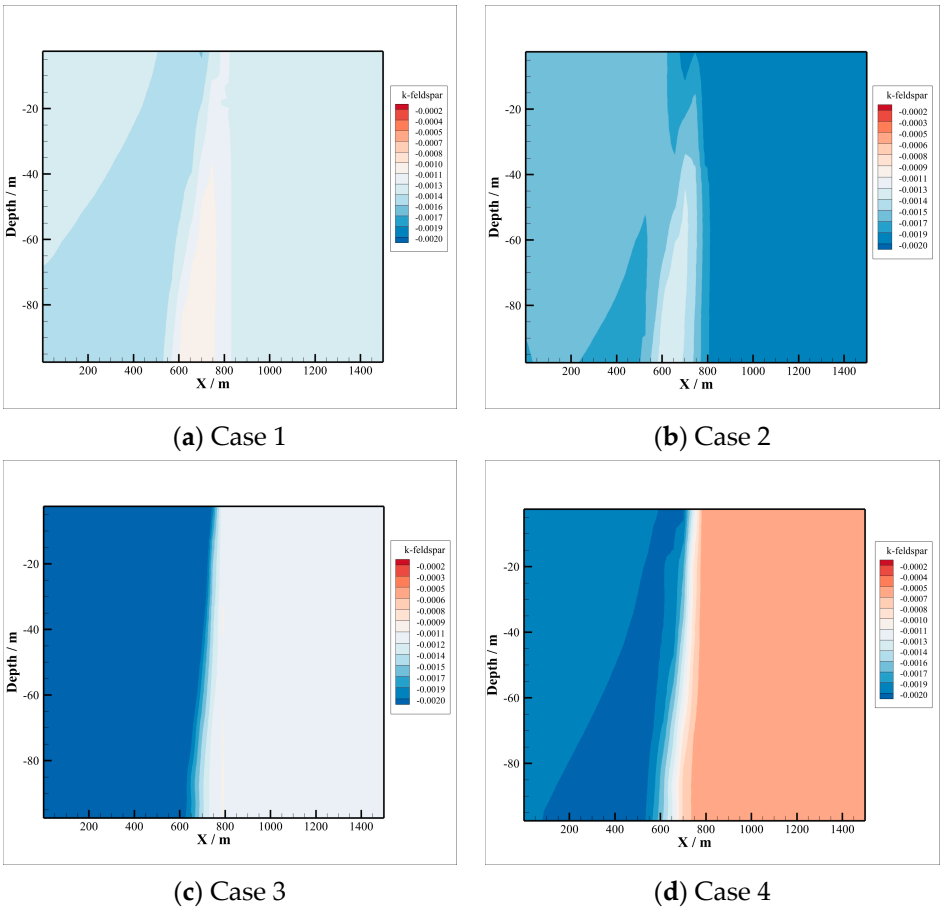

(**a**) Case 1 (**b**) Case 2

(**c**) Case 3 (**d**) Case 4

Figure 13. K-feldspar dissolution in different cases.

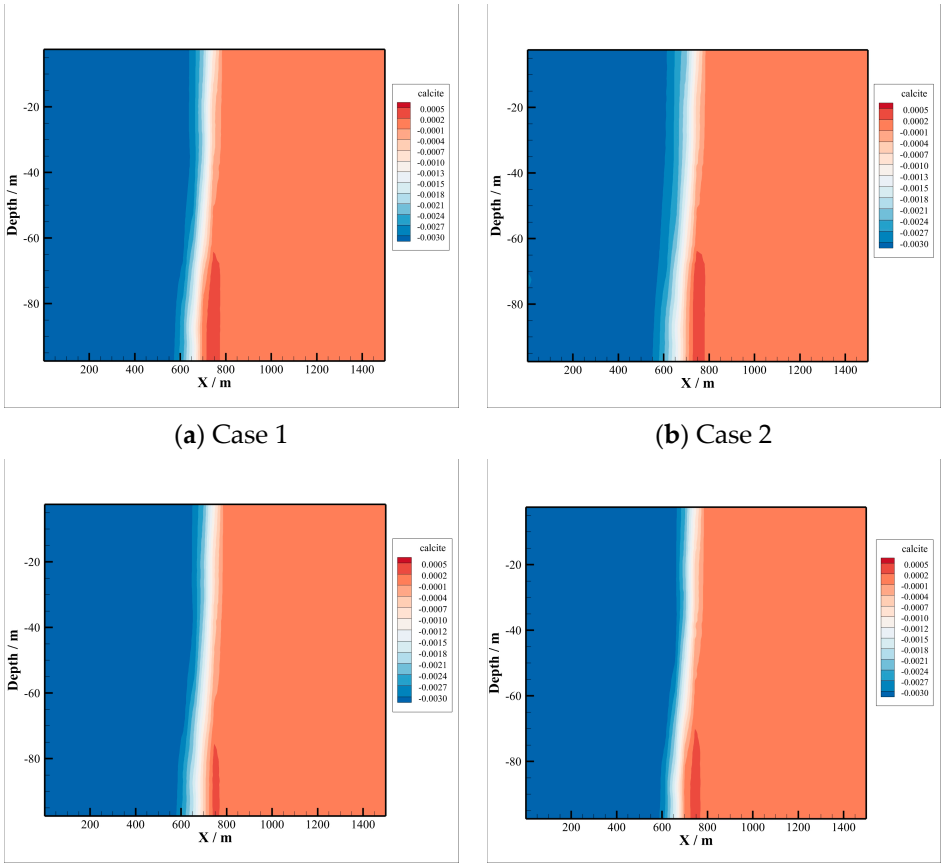

(**a**) Case 1 (**b**) Case 2

(**c**) Case 3 (**d**) Case 4

Figure 14. Calcite dissolution in different cases.

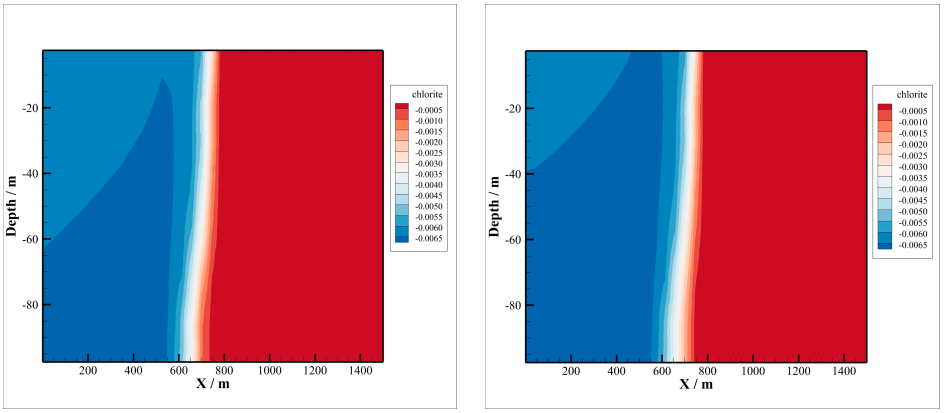

(**a**) Case 1 (**b**) Case 2

Figure 15. *Cont.*

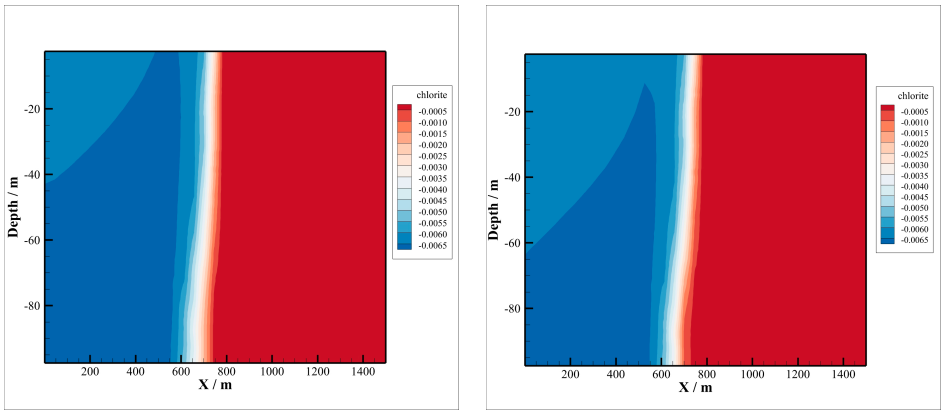

(**c**) Case 3 (**d**) Case 4

Figure 15. Chlorite dissolution in different cases.

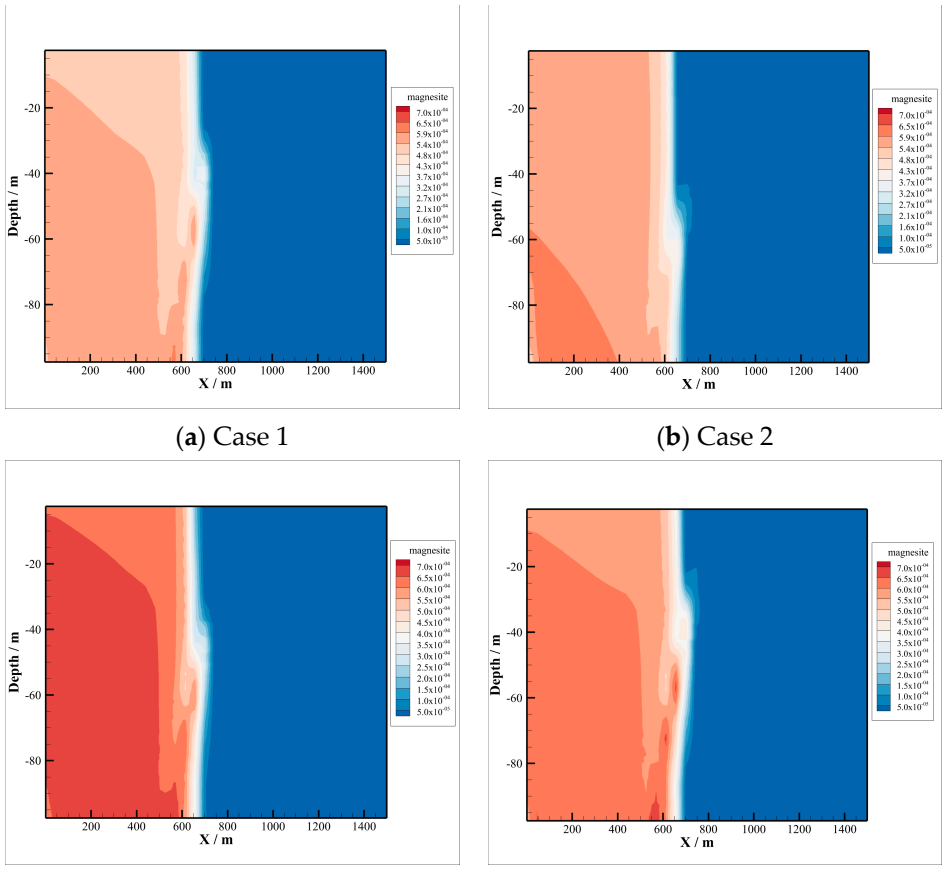

(**a**) Case 1 (**b**) Case 2

(**c**) Case 3 (**d**) Case 4

Figure 16. Magnesite precipitation in different cases.

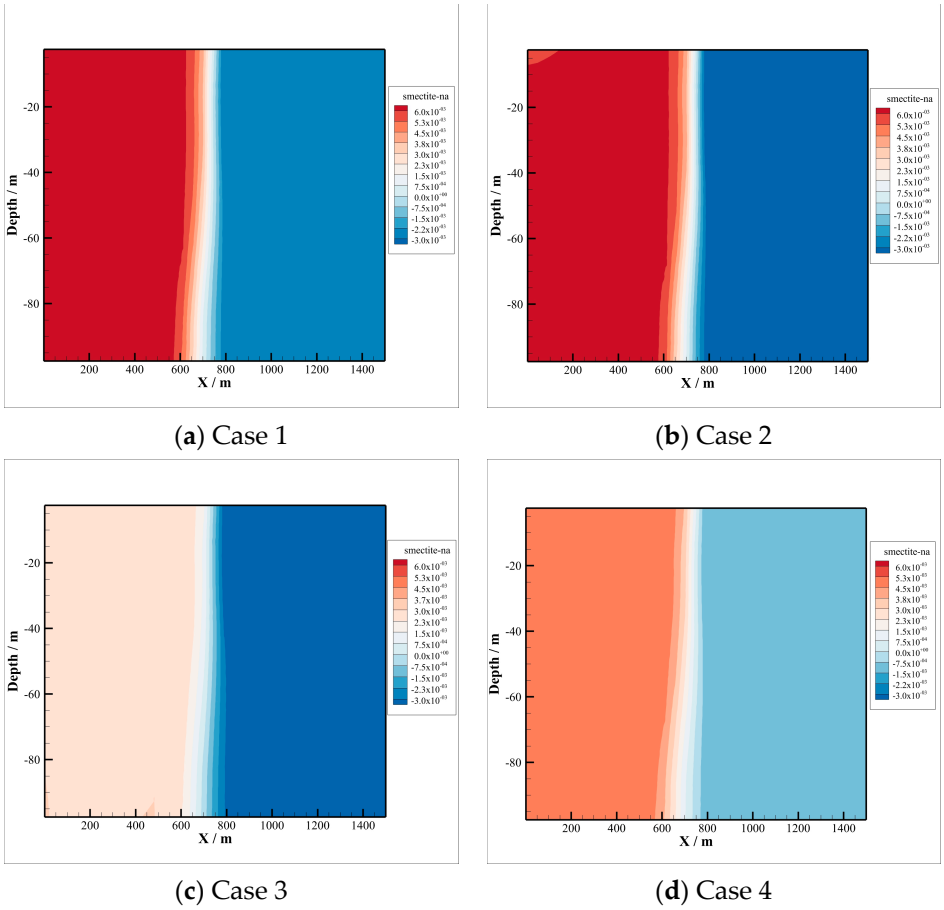

(**a**) Case 1 (**b**) Case 2

(**c**) Case 3 (**d**) Case 4

Figure 17. Smectite-Na precipitation in different cases.

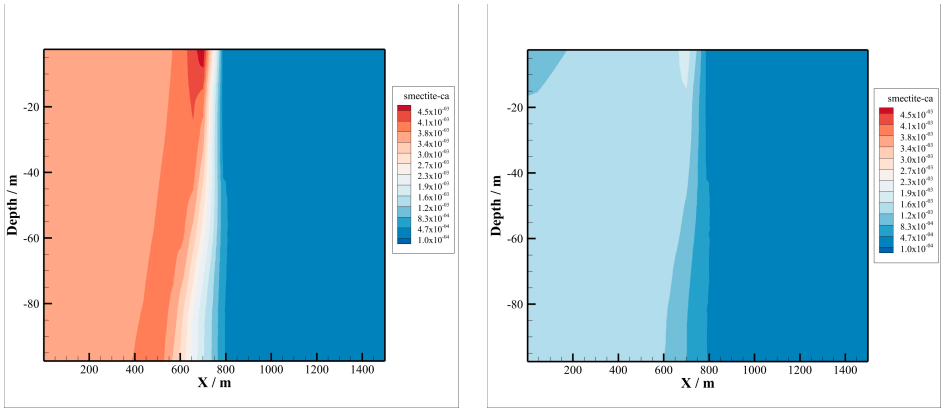

(**a**) Case 1 (**b**) Case 2

Figure 18. *Cont*.

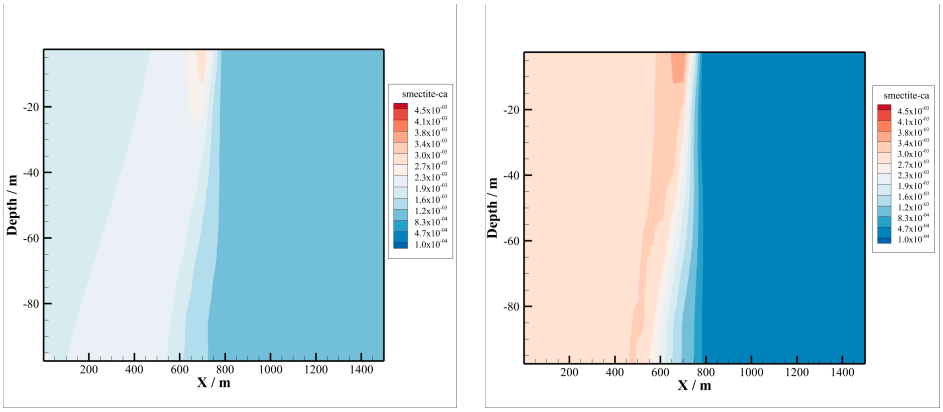

(**c**) Case 3 (**d**) Case 4

Figure 18. Smectite-Ca precipitation in different cases.

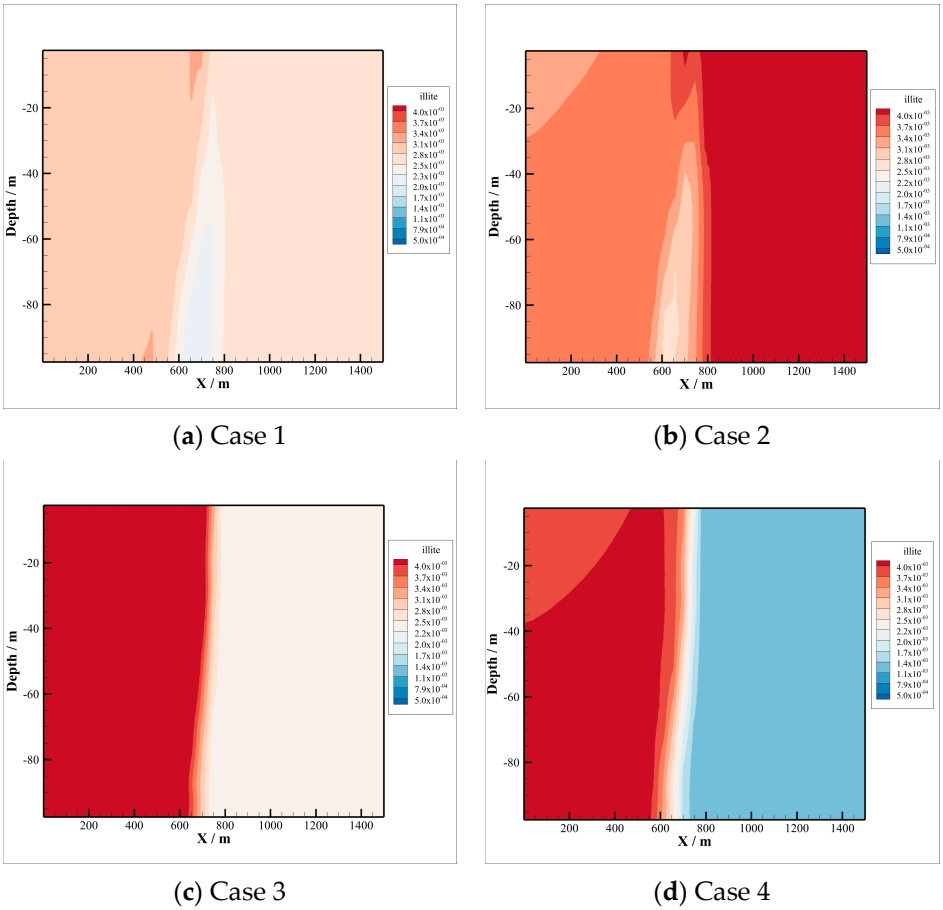

(**a**) Case 1 (**b**) Case 2

(**c**) Case 3 (**d**) Case 4

Figure 19. Illite precipitation in different cases.

For K-feldspar dissolution reaction, the higher the content, the greater the dissolution, as shown in Figure 13. Because of both K-feldspar and albite generating AlO_2^-, there will be a common ion effect. Therefore, the degree of K-feldspar dissolution in Case 2 is greater than in Case 1, as shown in Figure 13a,b. The reason is that the albite content in the latter case is almost twice the value of the first case. There is much more K-feldspar dissolution in Cases 3 and 4 than in Cases 1 and 2, because of the greater content than in Cases 3 and 4, as depicted in Figure 13c,d.

The contents of calcite in four cases are almost the same, as well as chlorite. There is little difference in the amount of dissolution of both calcite and chlorite, which can be found in both Figures 14 and 15. Chlorite dissolution will produce large amounts of Mg^{2+}, Al^{3+}, and AlO_2^-. Mg^{2+} is the main source of magnesite, smectite-Na, and smectite-Ca precipitation, as shown in Figures 16–18, respectively. Al^{3+} is the main source for smectite-Na and smectite-Ca precipitation.

The amount of smectite-Na precipitation is proportional to the content of albite. The largest amount of smectite-Na precipitation appears in Figure 17a, and the least amount appears in Figure 17c. For smectite-Ca precipitation, the largest amount appears in Case 1, as shown in Figure 18, which corresponds to the least amount of illite precipitation. The reason for the smallest illite precipitation in Case 1, to some extent, is that smectite-Ca takes up more Mg^{2+} and Al^{3+}.

Illite precipitate is also an important secondary mineral in CO_2-brine-rock interactions. From Figure 19, we can see that Case 3 has the largest amount of illite precipitation, and the next is Case 4, both of which are proportional to the contents of K-feldspar, as listed in Table 2.

For different compositions of the reservoir, the degree of minerals dissolution may vary as well as minerals precipitation, which may lead to a different variation tendency. On the one hand, the porosity will increase first due to minerals dissolution after CO_2 injection into the reservoir, which results from the lower pH value of brine because of the acidity of CO_2. On the other hand, the porosity will then decrease due to the formation of secondary minerals in the CO_2-brine-rock reaction, resulting in precipitation. Therefore, the change in reservoir porosity results from two reactions: primary mineral dissolution and secondary mineral precipitation. As shown in Figures 20 and 21, the porosity and permeability change in different cases. The overall trends are similar. The decrements of Case 2 and Case 3 are larger than those of the other two cases. Case 1 and Case 4 are almost the same. These differences may be associated with anorthite and K-feldspar dissolution. The sum of the two feldspar determines the decrease in porosity and the permeability. For CO_2 geological sequestration, mineralization will consume vast quantities of CO_2 regardless of the matter dissolution or precipitation. The process is of positive significance to safe CO_2 sequestration, which is regarded as the safest storage mechanism.

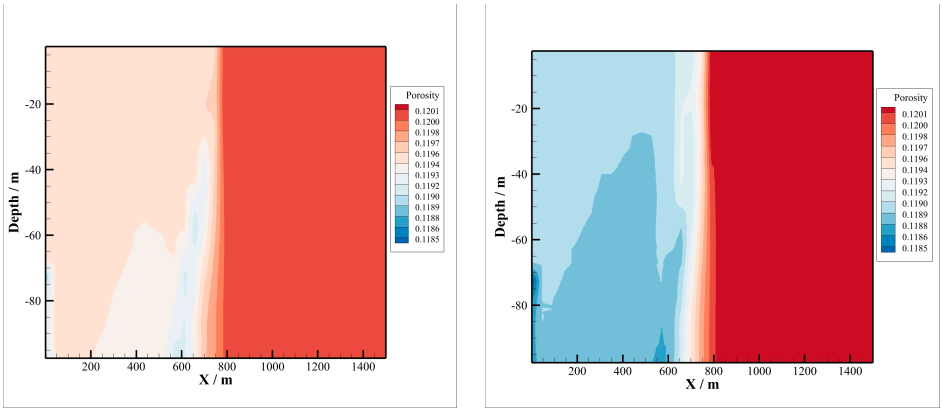

(**a**) Case 1 (**b**) Case 2

Figure 20. *Cont.*

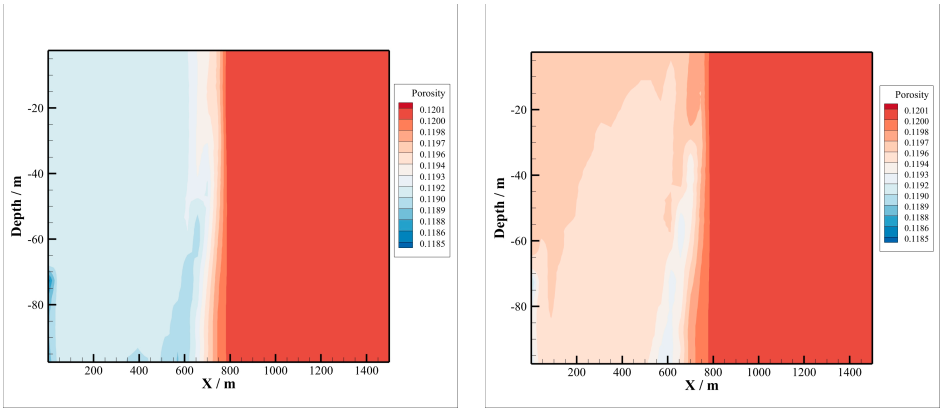

(**c**) Case 3 (**d**) Case 4

Figure 20. Porosity variations in different cases.

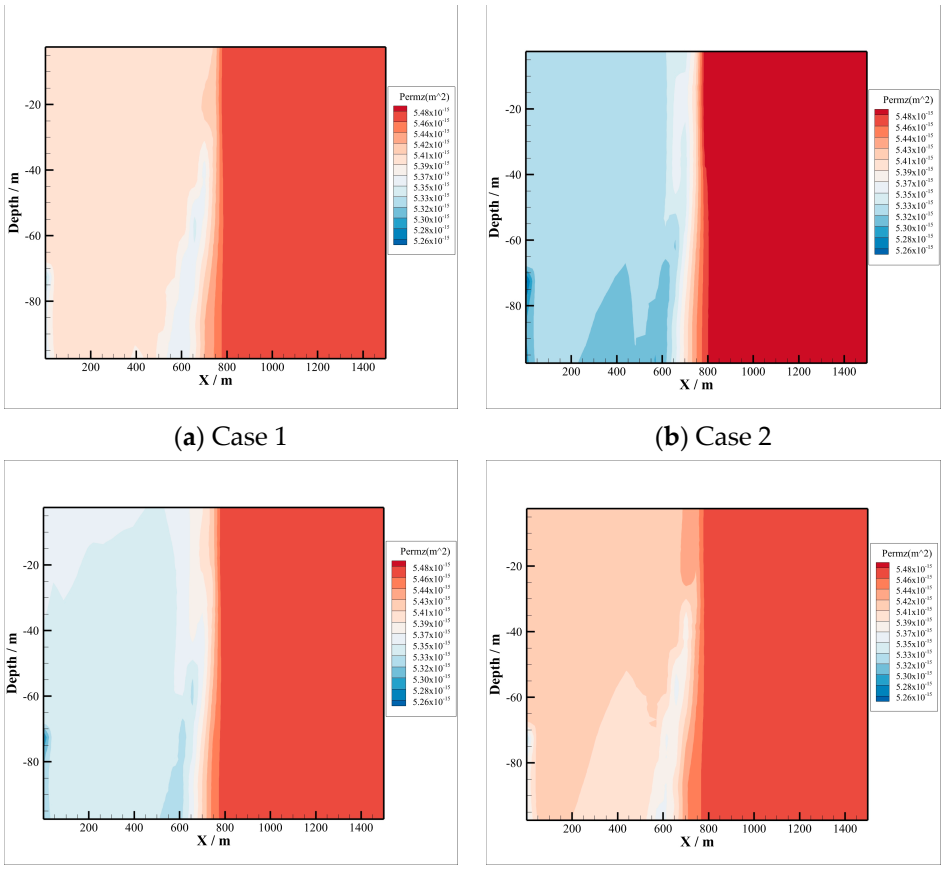

(**a**) Case 1 (**b**) Case 2

(**c**) Case 3 (**d**) Case 4

Figure 21. Permeability variations in different cases.

4. Conclusions

The process of CO_2 sequestration will have significant impacts on the geochemical properties and physical parameters of the reservoir. During CO_2 injection, the largest factor affecting the security of storage is the rapidly increasing pressure brought by gas injection. The gas saturation in the reservoir reaches the maximum around the injection well at the end of the injection period, which is the time node with the highest probability of reservoir risk. After that, CO_2 will migrate horizontally. The spreading width may be several kilometers; however, the risk of leakage may be reduced. During the long storage

life after injection, the CO_2-brine-rock reaction driven by a large amount of CO_2 exerts the greatest influence on the reservoir physical properties.

Carbonation is the most important one among all interactions according to the numerical simulation. The acidized brine will promote CO_2-brine-rock interactions because of CO_2 dissolution. The lower pH will increase the reaction rate, and the reaction will buffer the pH value of acidized brine. Feldspar, calcite, and chlorite will dissolve once CO_2 is injected into the reservoir. Magnesite, illite, smectite, siderite, and ankerite will precipitate after the beginning of the dissolution. Minerals dissolution will provide cations for secondary minerals precipitation. To analyze the sensitivity of numerical simulation, we also set four cases to investigate the mineral contents effect on the reaction. The results show that there is competition among ions. One mineral may precipitate first, which may result in another mineral precipitation decrease.

Moreover, the CO_2-brine-rock interaction occurring after CO_2 injection can alter the physical property distribution of the reservoir. From the simulation results, the porosity of the reservoir increases first and then decreases on long-term CO_2 sequestration, which is closely related to the geochemical reaction of the main minerals. On the contrary, mineral components of the reservoir are of great significance to the mineralization of CO_2. Regardless of the mineral dissolution or precipitation, they all play important roles in the long-term safe storage of CO_2. On the one hand, these interactions will promote CO_2 dissolution and reduce leakage risk; on the other hand, secondary minerals in the CO_2-brine-rock reaction can permanently sequester CO_2 in the reservoir. Although the reaction rate is very slow, it is the most ideal storage mechanism from the perspective of storage safety.

Author Contributions: Conceptualization, Z.L. and Y.L.; methodology, X.F.; software, B.L.; formal analysis, B.L.; investigation, Z.L.; resources, X.F.; writing—original draft preparation, Z.L. and B.L.; visualization, B.L.; supervision, Y.L.; project administration, B.L. All authors have read and agreed to the published version of the manuscript.

Funding: This research was funded by the CNPC Innovation Fund, grant number 2021DQ02-1103; National Key Research and Development Program, grant number SQ2022YFE020862; National Natural Science Foundation of China, grant numbers 41602134 and 42072166.

Data Availability Statement: The data presented in this study are available on request from the corresponding author. The data are not publicly available due to privacy.

Conflicts of Interest: The authors declare no conflict of interest.

References

1. Wang, W.; Wang, S.; Ma, X. Recent advances in catalytic hydrogenation of carbon dioxide. *Chem. Soc. Rev.* **2011**, *40*, 3703–3727. [CrossRef] [PubMed]
2. Wei, J.; Ge, Q.; Yao, R.; Wen, Z.; Fang, C.; Guo, L.; Xu, H.; Sun, J. Directly converting CO_2 into a gasoline fuel. *Nat. Commun.* **2017**, *8*, 15174. [CrossRef] [PubMed]
3. Aliev, F.; Mirzaev, O.; Kholmurodov, T.; Slavkina, O.; Vakhin, A. Utilization of Carbon Dioxide via Catalytic Hydrogenation Processes during Steam-Based Enhanced Oil Recovery. *Processes* **2022**, *10*, 2306. [CrossRef]
4. Bachu, S.; Adams, J.J. Sequestration of CO_2 in geological media in response to climate change: Capacity of deep saline aquifers to sequester CO_2 in solution. *Energy Convers. Manag.* **2003**, *44*, 3151–3175. [CrossRef]
5. Bachu, S.; Bonijoly, D.; Bradshaw, J.; Burruss, R.; Holloway, S.; Christensen, N.P.; Mathiassen, O.M. CO_2 storage capacity estimation: Methodology and gaps. *Int. J. Greenh. Gas Control* **2007**, *1*, 430–443. [CrossRef]
6. Luo, A.; Li, Y.; Chen, X.; Zhu, Z.; Peng, Y. Review of CO_2 sequestration mechanism in saline aquifers. *Nat. Gas Ind. B* **2022**, *9*, 383–393. [CrossRef]
7. Jafari, M.; Cao, S.C.; Jung, J. Geological CO_2 sequestration in saline aquifers: Implication on potential solutions of China's power sector. *Resour. Conserv. Recycl.* **2017**, *121*, 137–155. [CrossRef]
8. Zhang, G.; Ranjith, P.G.; Fu, X.; Li, X. Pore-fracture alteration of different rank coals: Implications for CO_2 sequestration in coal. *Fuel* **2021**, *289*, 119801. [CrossRef]
9. Mitiku, A.B.; Li, D.; Bauer, S.; Beyer, C. Geochemical modelling of CO_2–water–rock interactions in a potential storage formation of the North German sedimentary basin. *Appl. Geochem.* **2013**, *36*, 168–186. [CrossRef]
10. Wu, X. *Carbon Dioxide Capture and Geological Storage the First Massive Exploration in China*; Science Press: Beijing, China, 2013; pp. 161–169.

11. Wang, T.; Wang, H.; Zhang, F.; Xu, T. Simulation of CO_2–water–rock interactions on geologic CO_2 sequestration under geological conditions of China. *Mar. Pollut. Bull.* **2013**, *76*, 307–314. [CrossRef]
12. Qu, X.; Liu, L.; Hu, D.; Ma, R.; You, L. Study on the Dawsonite Sandstones Reformation with CO_2 Fluid. *J. Jilin Univ. (Earth Sci. Ed.)* **2007**, *37*, 690–697.
13. Shen, X.; Liu, H.; Zhang, Y.; You, L.; Guo, M.; Ma, L. An integrated model for carbon geo-sequestration considering gas leakage. *J. Pet. Sci. Eng.* **2022**, *217*, 110899. [CrossRef]
14. Bie, H.; Yang, C.; Liu, P. Probabilistic evaluation of above-zone pressure and geochemical monitoring for leakage detection at geological carbon sequestration site. *Comput. Geosci.* **2019**, *125*, 1–8. [CrossRef]
15. Postma, T.J.W.; Bandilla, K.W.; Celia, M.A. Estimates of CO_2 leakage along abandoned wells constrained by new data. *Int. J. Greenh. Gas Control* **2019**, *84*, 164–179. [CrossRef]
16. Bateman, K.; Rochelle, C.A.; Purser, G.; Kemp, S.J.; Wagner, D. Geochemical Interactions Between CO_2 and Minerals within the Utsira Caprock: A 5-year Experimental Study. *Energy Procedia* **2013**, *37*, 5307–5314. [CrossRef]
17. Chen, X.; Li, Y.; Tang, X.; Qi, H.; Sun, X.; Luo, J. Effect of gravity segregation on CO_2 flooding under various pressure conditions: Application to CO_2 sequestration and oil production. *Energy* **2021**, *226*, 120294.
18. Ding, J.; Yan, C.; He, Y.; Wang, C. Supercritical CO_2 sequestration and enhanced gas recovery in tight gas reservoirs: Feasibility and factors that influence efficiency. *Int. J. Greenh. Gas Control* **2021**, *105*, 103234. [CrossRef]
19. Sun, X.; Bi, Y.; Guo, Y.; Ghadiri, M.; Mohammadinia, M.S. CO_2 geo-sequestration modeling study for contact angle estimation in ternary systems of brine, CO_2, and mineral. *J. Clean. Prod.* **2021**, *283*, 124662. [CrossRef]
20. Xu, T.; Sonnenthal, E.; Spycher, N.; Pruess, K. TOUGHREACT—A simulation program for non-isothermal multiphase reactive geochemical transport in variably saturated geologic media: Applications to geothermal injectivity and CO_2 geological sequestration. *Comput. Geosci.* **2006**, *32*, 145–165. [CrossRef]
21. Lasaga, A.; Soler, J.; Ganor, J.; Burch, T.; Nagy, K. Chemical weathering rate laws and global geochemical cycles. *Geochim. Et Cosmochim. Acta* **1994**, *58*, 2361–2386. [CrossRef]
22. Tian, H. Impacts of CO_2-Brine-Rock Interaction on the Caprock Sealing Efficiency: A Case Study of Shiqianfeng Formation Mudstone Caprock in Ordos Basin. PhD Thesis, Jilin University, Changchun, China, 2014.
23. Zhang, F.; Wang, H.; Wang, H.; Wang, G.; Yang, X.; Wang, T. Experiment on mechanism of CO_2 fluid interacting with sandstone layer. *J. Jilin Univ. (Earth Sci. Ed.)* **2012**, *42*, 821–826.